Pharmacological Reports (2020) 72:692–704
https://doi.org/10.1007/s43440-020-00070-w

ARTICLE

Synthesis, molecular modelling and biological activity of some pyridazinone derivatives as selective human monoamine oxidase-B inhibitors

Zeynep Özdemir[1] · Mehmet Abdullah Alagöz[1] · Harun Uslu[2] · Arzu Karakurt[1] · Acelya Erikci[3] · Gulberk Ucar[3] · Mehtap Uysal[4]

Received: 18 October 2019 / Revised: 3 January 2020 / Accepted: 8 January 2020 / Published online: 6 March 2020

Abstract

Background Since brain neurotransmitter levels are associated with the pathology of various neurodegenerative diseases like Parkinson and Alzheimer, monoamineoxidase (MAO) plays a critical role in balancing these neurotransmitters in the brain. MAO isoforms appear as promising drug targets for the development of central nervous system agents. Pyridazinones have a broad array of biological activities. Here, six pyridazinone derivatives were synthesized and their human monoamine oxidase inhibitory activities were evaluated by molecular docking studies, in silico ADME prediction and in vitro biological screening tests.

Methods The compounds were synthesized by the reaction of different piperazine derivatives with 3 (2*H*)-pyridazinone ring and MAO-inhibitory effects were investigated. Docking studies were conducted with Maestro11.8 software.

Results Most of the synthesized compounds inhibited hMAO-B selectively except compound **4f**. Compounds **4a–4e** inhibited hMAO-B selectively and reversibly in a competitive mode. Compound **4b** was found as the most potent ($k_i = 0.022 \pm 0.001$ µM) and selective (SI ($Ki_{\text{hMAO-A/hMAO-B}}$) = 206.82) hMAO-B inhibitor in this series. The results of docking studies were found to be consistent with the results of the in vivo activity studies. Compounds **4a–4e** were found to be non-toxic to HepG2 cells at 25 µM concentration. In silico calculations of ADME properties indicated that the compounds have good pharmacokinetic profiles.

Conclusion It was concluded that 4b is possibly recommended as a promising nominee for the design and development of new pyridazinones which can be used in the treatment of neurological diseases.

Electronic supplementary material The online version of this article (https://doi.org/10.1007/s43440-020-00070-w) contains supplementary material, which is available to authorized users.

✉ Zeynep Özdemir
zeynep.bulut@inonu.edu.tr; zpozdmr@gmail.com

[1] Department of Pharmaceutical Chemistry, Faculty of Pharmacy, Inonu University, 44280 Malatya, Turkey

[2] Department of Anesthesiology, Vocational School of Health Services, Fırat University, 23119 Elazığ, Turkey

[3] Department of Biochemistry, Faculty of Pharmacy, Lokman Hekim University, 06510 Ankara, Turkey

[4] Department of Pharmaceutical Chemistry, Faculty of Pharmacy, Gazi University, 06100 Ankara, Turkey

Graphic abstract

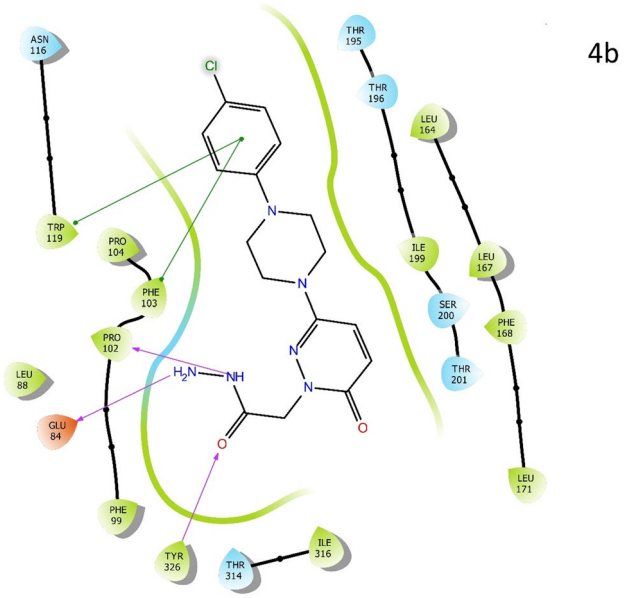

Keywords Pyridazinone · Monoamine oxidase inhibition · Molecular docking

Introduction

Monoamine oxidase (MAO) is a flavin adenine dinucleotide (FAD)-dependent enzyme located mainly in the mitochondrial membrane of CNS and peripheral tissues which is responsible for the metabolism of neurotransmitters such as dopamine (DA), serotonin (5-HT), adrenaline (E), and noradrenaline (NE) and for the inactivation of exogenous arylalkyl amines. MAO exists in two isoforms such as MAO-A and -B, which show high sequence similarity, but exhibit different tissue distribution as well as different substrate and inhibitor specificities. MAO-A displays a higher affinity for 5-HT and NE, while MAO-B prefers phenylethyl amine (PEA). Although the metabolisms of DA, tryptamine and tyramine are generated by both isoforms, DA is mainly degraded by MAO-A in the rodent brain, while MAO-B is responsible for the metabolism of DA in humans. MAO-A is selectively inhibited by clorgyline, whereas MAO-B is inhibited by selegiline (l-deprenyl) [1, 2].

Since brain neurotransmitter levels are associated with the pathology of various neurological diseases including Parkinson's disease (PD) and Alzheimer's disease (AD), and MAO plays a critical role in the regulation of these neurotransmitters in brain, MAO isoforms appear as promising drug targets for the development of CNS agents. Reversible and irreversible monoamine oxidase inhibitors (MAOIs) are previously developed, and are currently in use clinically for the treatment of psychological–neurological disorders [3]. And also, the use of MAOIs is limited due to undesirable drug–food and drug–drug interactions and also due to their adverse effects. Therefore, extensive efforts have been devoted to the discovery of novel selective and reversible MAO inhibitors to avoid their undesirable side effects. Selective MAO-A inhibitors are generally developed for the management of depression and anxiety disorders whereas selective MAO-B inhibitors are designed for the treatment of PD and AD with a better safety profile as compared to nonselective MAO inhibitors [4–8].

MAO inhibitors have different structures such as pyrazoline, carboline, cyclopropylamine, hydrazine, hydrazide, indolalkylamine, oxazolidinone benzothiazinone, coumarin, safinamide, chromone, anilide and propargylamine [9–12]. Among them, substituted hydrazines and hydrazides, particularly thiazolylhydrazine derivatives have previously been described as effective MAOIs showing inhibitory effects at different micromolar concentrations [11, 13]. Pyridazinone is a six-membered heterocycle which has two contiguous nitrogen atoms, one carbonyl within the ring, and one endocyclic double bond. Due to this structure, it is considered as cyclic hydrazine. Pyridazinones have a broad array of biological activities including antibacterial, analgesic, antinociceptive, anticonvulsant, antiinflammatory, antianemic, diuretic, antiasthmatic, antisecretory, insecticidal antidepressant, antihypertensive, cardiotonic, anti-cancer, and antiulcer properties [14–25].

As the pyridazinone ring structure also has a cyclic hydrazide group which has been shown earlier to have MAO-inhibitory activity, some 6-substitute-3(2*H*)-pyridazinone derivatives were designed, synthesized and potential MAO-inhibitory activities were evaluated. The 6th position of pyridazinone was taken into consideration when making changes in cognitive structures. Phenyl, substituted phenyl, benzyl, and other groups are added as substituents in different positions of this the ring. The interactions of compounds with the human MAO (hMAO) isoforms were performed using molecular docking approach. MAO inhibition effects on synthesized molecules were determined by recombinant hMAO isoforms. Since ADMET properties of compounds are important parameters for determining their druglike properties, and it has been reported that early estimation of ADMET in the discovery phase reduces dramatically the fraction of pharmacokinetics-related failure in the clinical phases and saves the time and cost, the designed compounds (**4a**–**4f**) were submitted to the ADMET SAR web-server to perform an in silico analysis of pharmacokinetic parameters and determine the ADMET properties.

Materials and methods

Chemistry

Synthesis starting compounds were obtained from Aldrich and E. Merck. Starting materials were synthesized according to a previous method [17, 19, 26]. The impurities were checked with TLC. Melting points of compounds were determined using an electrothermal device. IR spectral data were obtained by ATR technique using Perkin Elmer Spectrometer ^{1}H-NMR. ^{13}C-NMR spectra were obtained using Brucker Avonce Ultrashield FT-NMR spectrometer at 300 MHz and 75 MHz, respectively, in DMSO. LC/MSMS spectra were recorded on Agilent 6400 Series. Triple quadrupole elemental analysis of the compounds was carried out using Leco CHNS-932. All analyses were conducted in the central research laboratory of Inonu University.

Synthesis of starting compounds (1a–f, 2a–f, 3a–f)

To obtain **1a–f**, 0.01 mol of substituted piperazine/piperidine and 0.01 mol of 3,6-dichloropyridazine were dissolved in 15 ml EtOH, it was stirred under reflux for 6 h. And then, the medium was transferred to ice water. The solid formed was filtered and purified by crystallization with ethanol.

To obtain **2a–f**, 0.05 mol of 6-substituted-3-chloropyridazinone derivative is dissolved in 30 ml of glacial acetic acid and was refluxed for 6 h. Acetic acid is removed from the reaction medium with a rotary evaporator. Residue was added to water and then the extraction is carried out with chloroform. Chloroform phase is separated with sodium sulfate, the chloroform is removed under reduced pressure. The residue was purified by crystallization in ethanol.

To obtain **3a–f**, 0.01 mol of 6-substituted-3(2*H*)-pyridazinone, 0.02 mol of ethyl bromoacetate, and 0.02 mol of potassium carbonate in 40 ml of acetone were prepared. The mixture was refluxed for about 12 h. The mixture was cooled after reflux. The organic salts were removed by filtration. Acetone in the reaction medium was removed by evaporation. The residue was crystallized in methanol. The melting points of the synthesized compounds were compared with the melting points of the substances registered in the literature [18, 19, 26–29].

Synthesis of title compounds (4a–f)

0.01 mol of ethyl 6-substituted-3(2*H*)-pyridazinone-2-ylacetate was added to 25 ml of methanol. 3 ml of 99% hydrazine hydrate solution was added to this mixture and stirred at room temperature for 3 h. The reaction medium was filtered, the solid obtained was washed with water and dried. The residue was crystallized with ethanol to be purified. The melting points of the synthesized compounds were compared with the melting points of the substances registered in the literature [18, 19, 26–29]. The spectral data of the newly synthesized compound **4e** are given below. The structure of the compound is in agreement with the spectral data.

6-[4-(Ethoxycarbonyl) piperazine-1-yl]-3(2*H*)-pyridazinone-2-yl acetohydrazide (4e)

White crystals; yield: 79.23%; mp: 253–4 °C; IR (cm^{-1}, ATR): 3489 (N–H), 3168 (C–H aromatic), 2864 (C–H), 1676 (C=O), 1590 (C=N) and 1241 (C–N); ^{1}H-NMR ($CDCl_3$–*d*, 300 MHz): δ (ppm)1.29 (3H; *t*; $–OCH_2C\underline{H}_3$), 3.27 (4H; *t*; $C\underline{H}_2–N$), 3.57 (4H; *t*; $C\underline{H}_2–N$), 4.15–4.18 (2H; *q*; $–OCH_2C\underline{H}_3$), 4.69 (2H; *s*; $–N–CH_2–C=O$), 4.84 (2H; *s*; $–NH_2$), 6.92 (1H; *d*; pyridazinone H^5), 7.19 (1H; *d*; pyridazinone H^4) and 7.93 (1H; *s*; –NH–N). ^{13}C-NMR (100 MHz), δ14.65 (1C; $–OCH_2\underline{C}H_3$), 43.00 (2C; $CH_2–N$), 46.39 (2C; $CH_2–N$), 54.62 (1C; $–N–\underline{C}H_2–C=O$), 61.68 (1C; $–O\underline{C}H_2CH_3$), 126.06 (1C; pyridazinone C^5), 131.24 (1C; pyridazinone C^4), 149.29 (1C; pyridazinone C^6), 155.41 (1C; $CH_2–N–\underline{C}=O$), 158.61 (1C; –O–C=O), and 168.08 (1C; pyridazinone C^3); LC/MSMS (ESI+) *m/z* 325.1 $[M+H]^+$; anal. Calcd. For $C_{13}H_{20}FN_6O_4$. H_2O: C, 45.61; H, 6.48; N, 24.55. Found: C, 45.21; H, 6.164; N, 24.25%.

Biological activity

MAO-inhibitory activity screening

The synthesized derivatives were investigated for their hMAO-inhibitory effects with recombinant hMAO-A and hMAO-B enzymes and Amplex Red MAO assay kit according to the manufacturer's instructions. Recombinant enzymes and the other chemicals were purchased from Sigma-Aldrich (Germany).

In the assay, MAO activity is measured continuously. Tyramine (0.05–0.50 mM) was used as the common substrate for MAO isoforms. Selegiline, lazabemide and moclobemide were used as specific MAO inhibitors. Fluorescence was measured using excitation at 530 nm and emission at 590 nm [30, 31].

Kinetic studies

To understand the mode of MAO inhibition, the synthesized molecules and reference inhibitors (*selegiline*: selective and irreversible MAO-B inhibitor, *lazabemide*: selective and reversible MAO-B inhibitor and *moclobemide* as selective and reversible MAO-A inhibitor) were dissolved inDMSO and prepared at concentrations of 0.001–20.00 µM. Results are shown with double reciprocal Lineweaver–Burk plots. SI values were calculated as Ki. Protein content of the samples was determined by Bradford's method (SIGMA Total Protein kit, Micro TP0100).

Reversibility

Reversibility was calculated with the dialysis method formerly reported [32]. Briefly, 16 × 25 mm of dialysis tubings with a molecular weight cut-off of 12 was used. Enzyme samples and the reference inhibitors were incubated with the compounds at a concentration fivefold of their K_i values for the inhibition of *h*MAO-A and –B at 37 °C. Samples were dialyzed two times in 24 h at 4 °C in dialysis buffer of 100 mM potassium phosphate, pH 7.4, 5% sucrose. Residual MAO activities were measured following dialysis.

In vitro blood–brain barrier permeation assay (PAMPA-BBB)

Since the blood–brain barrier (BBB) plays a major role in the diffusion of the drugs to the CNS, examination of drug transport through BBB is highly needed for the development of potential neuropharmaceuticals. Endothelial cell culture models of BBB are submitted as in vitro systems suitable for the procedures. Parallel artificial membrane permeability assay (PAMPA) is considered to be one of the most powerful physicochemical screening methods in CNS-targeted drug development. The PAMPA-BBB system mimics the rate of transcellular passive diffusion of drugs across the BBB by measuring the effective permeability (Pe, cm/s) of an artificial lipid membrane [33]. The assay was carried out in accordance with the instructions. (Pion Inc., USA) [34].

In vitro cytotoxicity

Cell viability was measured by a quantitative colorimetric assay with 3-[4,5 dimethylthiazol-2-yl]-2,5-diphenyltetrazolium bromide (MTT) (Sigma-Aldrich) [35]. Human hepatoma cell line HepG2 (Invitrogen) was used. MTT reduction was measured at 590 nm. Control cells treated with 0.1% DMSO were used at 100% viability [34]. Significance was determined using student's *t* test. Results were expressed as mean ± SEM. Differences are considered statistically significant at $p < 0.05$.

Molecular docking

The three-dimensional structures of compounds were constituted with Maestro11.8 software with the aid of MacroModel (Schrödinger, LLC, NY) software and the OPLS_2005 force field parameters, and were optimized by conjugated gradient method [36]. The ligand models were then ligated with LigPrep (Schrödinger, LLC, NY) software to determine the appropriate tautomeric and ionization states. The structures of MAO proteins retrieved from RCSB (www.rcsb.org) using the protein preparation wizard of Maestro for hMAO-A and 2Z5X, hMAO-B 4A79 PDB proteins [37]. Within this context, undesirable solvent molecules, ligands and segments in the crystal structures were deleted using Prime (Schrödinger, LLC, NY), Impact (Schrödinger, LLC, NY), Epic (Schrödinger, LLC, NY) and Propka softwares. The orientations of the polarized hydrogens and the water have been adjusted; hydrogen molecules were added and charges were assigned [38]. Grid maps of the binding sites of proteins were generated using Maestro's receptor grid-forming panel and the remaining ligands were ligated 40 times in standard precision mode using Glide (Schrödinger, LLC, NY) software [39–41]. The mean of the MAO's scores were calculated with visually examining anchor poses and taking into account the fit score of each of the ligaments determined for each ligand.

The receptor–ligand interactions were simulated and scored. Theoretical K_i value for each ligand was calculated with AutoDock 4.2 software [42, 43]. AutoDock4.2 software was used to clarify the interactions of molecules with hMAOs at molecular level. The compounds were docked to active sites of X-ray crystal structures of hMAO-A (PDB: 2Z5X) and hMAO-B (PDB:4A79) [43].

In silico ADMET

Screening of pharmacokinetic parameters and drug-likeness

The compounds were submitted for an in silico ADMET screening test to indicate the ADME properties of the synthesized derivatives. To have knowledge about whether the compounds planned to be synthesized can be pharmaceuticals, chemical bioavailability and optimum physical and chemical properties required for these compounds, Lipinski's rule of five, drug-likeness model score, total polar surface area (TPSA), miLog P, molecular volume (MV), number of rotatable bonds, number of hydrogen donor and acceptor atoms and aqueous solubility were calculated with software. The SMILES codes of the compounds were obtained for use in the Molinspiration software. Then some parameters were calculated by this software (https://www.molinspiration.com).

In silico ADMET prediction

The synthesized compounds were prepared in 2D Sketcher (Maestro, Schrodinger 11.8). The features (a set of ADMET-related properties which is a total of 46 molecular descriptors) were calculated using the QikProp program (Maestro, Schrodinger 11.8) running in normal mode. QikProp is an ADME estimation program that theoretically calculates the various parameters of molecules and uses them to compare them with those of 95% of known drugs.

Results

Chemistry

4a–f were synthesized according to the Scheme 1. Compound 4e has not yet been published. Molecular structure of this new compound was proved with ^{1}H-NMR, ^{13}C-NMR, LC/MSMS and elementary analyses. Molecular features of **4a–f** are given in Table 1.

Biological activity

MAO-inhibitory screening

Specific enzyme activities were calculated as 0.147 ± 0.009 nmol/mg/min ($n = 3$) for hMAO-A and 0.134 ± 0.007 nmol/mg/min ($n = 3$) for hMAO-B. All synthesized pyridazinones except compound **4f**, which inhibited the MAO isoforms non-selectively, inhibited hMAO-B selectively at low micromolar concentration ranges (Table 2).

Kinetic studies

Figure 1 shows inhibition of hMAO-B by compound **4b**, the most effective molecule in the series. The slopes of the Lineweaver–Burk plots were plotted versus the inhibitor concentration and the K_i value was determined from the x-axis intercept as $-K_i$. It has been shown that the lines are linear and intersect on the y-axis, which suggests that compound **4b** is a competitive inhibitor of hMAO-B (Fig. 1). Ki value was thought to be 0.023 µM.

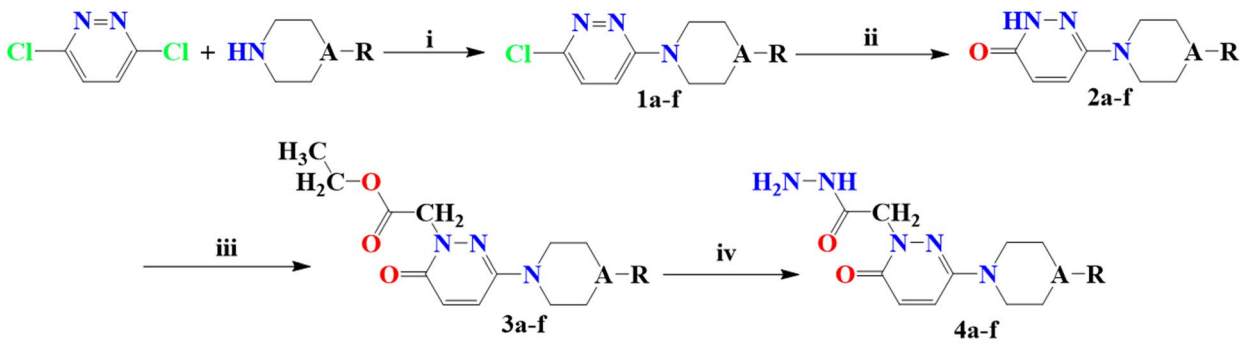

(i) EtOH, reflux (6h); (ii) AcOH, reflux (6h); (iii) $BrCH_2COOCH_2CH_3$, K_2CO_3, aceton, reflux (24h), (iv) $H_2NNH_2.H_2O$, MeOH, stirred in rt (3h)
A:; C/N
R; 4a: phenyl, 4b: 4-chlorophenyl, 4c: 3,4-dichlorophenyl, 4d: 2-fluorophenyl, 4e: ethoxy carbonyl, 4f: benzyl.

Scheme 1 Synthesis of the compounds

Table 1 Molecular structures, yields, melting points and molecular weights of **4a–f**

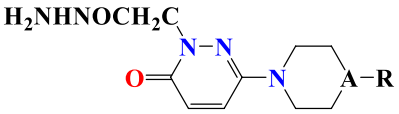

Compounds	A	R	Yield (%)	MP (°C)	MW (g/mol)	Molecular formula
4a	N	Phenyl	82	251–252	328.37	$C_{16}H_{20}N_6O_2$
4b	N	4-chlorophenyl	81	228–229	362.81	$C_{16}H_{19}ClN_6O_2$
4c	N	3,4-dichlorophenyl	78	207–208	397.26	$C_{16}H_{18}Cl_2N_6O_2$
4d	N	2-fluorophenyl	79	253–254	346.36	$C_{16}H_{19}FN_6O_2$
4e	N	Ethoxy carbonyl	60	258–259	324.34	$C_{13}H_{20}N_6O_4$
4f	C	Benzyl	75	218–219	341.41	$C_{18}H_{23}N_5O_2$

Table 2 Calculated and experimental K_i values for the inhibition of hMAO isoforms by the synthesized pyridazinone derivatives

Compounds	Calculated K_i hMAO-A) [μM]	Calculated K_i (hMAO-B) [μM]	SI	Selectivity	Experimental K_i (hMAO-A) [μM]	Experimental K_i (hMAO-B) [μM]	SI	Inhibition type	Selectivity
4a	1.95	0.106	18.40	MAO-B	2.200 ± 0.015	0.055 ± 0.002	40.00	Competitive	MAO-B
4b	2.24	0.071	31.55	MAO-B	4.550 ± 0.241	0.022 ± 0.001	206.82	Competitive	MAO-B
4c	1.53	0.108	14.17	MAO-B	1.820 ± 0.110	0.050 ± 0.002	36.40	Competitive	MAO-B
4d	1.18	0.117	10.09	MAO-B	2.167 ± 0.140	0.061 ± 0.003	35.52	Competitive	MAO-B
4e	4.13	0.800	5.16	MAO-A	4.220 ± 0.147	0.744 ± 0.030	5.67	Competitive	MAO-B
4f	1.27	0.633	2.01	MAO-B	1.045 ± 0.002	0.997 ± 0.043	1.05	Competitive	Non-selective
Selegiline	**29.34**	**23.73**	**1.24**	**MAO-B**	**17.000 ± 1.125**	**0.220 ± 0.013**	**77.27**	**Suicide inhibitor**	**MAO-B**
Lazabemide	**264.11**	**21.23**	**12.44**	**MAO-B**	**3200.00 ± 55.000**	**0.004 ± 0.001**	**800.00**	**Competitive**	**MAO-B**
Moclobemide	**1.87**	**2.64**	**0.71**	**MAO-A**	**0.013 ± 0.001**	**1.95 ± 0.12**	**0.007**	**Competitive**	**MAO-A**

Each value represents the mean ± SEM of three independent experiments. The selectivity index (SI) was calculated as K_i(MAO-A)/K_i (MAO-B). Selectivity towards MAO-A increases as the corresponding SI decreases while selectivity towards MAO-B isoform increases as the corresponding SI increases

Reversibility

The present test showed that selegiline, a wellknown suicide inhibitor of MAO-B appeared as irreversible inhibitor since the residual hMAO-B activity was not recovered after dialysis (Table 3). On incubation with lazabemide, the remaining hMAO-B activity was found to be13.00 ± 1.01%. The enzyme activity was recovered up to 96.87 ± 2.97% after dialysis indicating that lazabemide is a reversible inhibitor of hMAO-B.

Blood–brain barrier permeation

The synthesized derivatives were screened for their ability to cross the blood–brain barrier (BBB) since getting drugs across BBB is a key for the design and development of more successful therapies to treat CNS disorders, like Alzheimer's disease and depression.

To investigate whether the present compounds could pass this barrier, PAMPA-BBB was used. Assay validation was made by comparing experimental permeabilities of nine commercial drugs with reported values (Table 4). A plot of experimental data versus reference values gave a good linear correlation (R^2 = 0.997). According to the limits reported earlier [34] for BBB permeation, compounds were classified as follows:

CNS + (high BBB permeation predicted): Pe $\left(10^{-6}\text{cm s}^{-1}\right) > 4.00$,

CNS − (low BBB permeation predicted): Pe $\left(10^{-6}\text{cm s}^{-1}\right) < 2.00$,

CNS ± (BBB permeation uncertain)

: Pe $\left(10^{-6}\text{cm s}^{-1}\right)$ from 4.00 to 2.00.

The data showed that all of the novel pyridazinone derivatives can cross the BBB successfully. Compounds **4b**

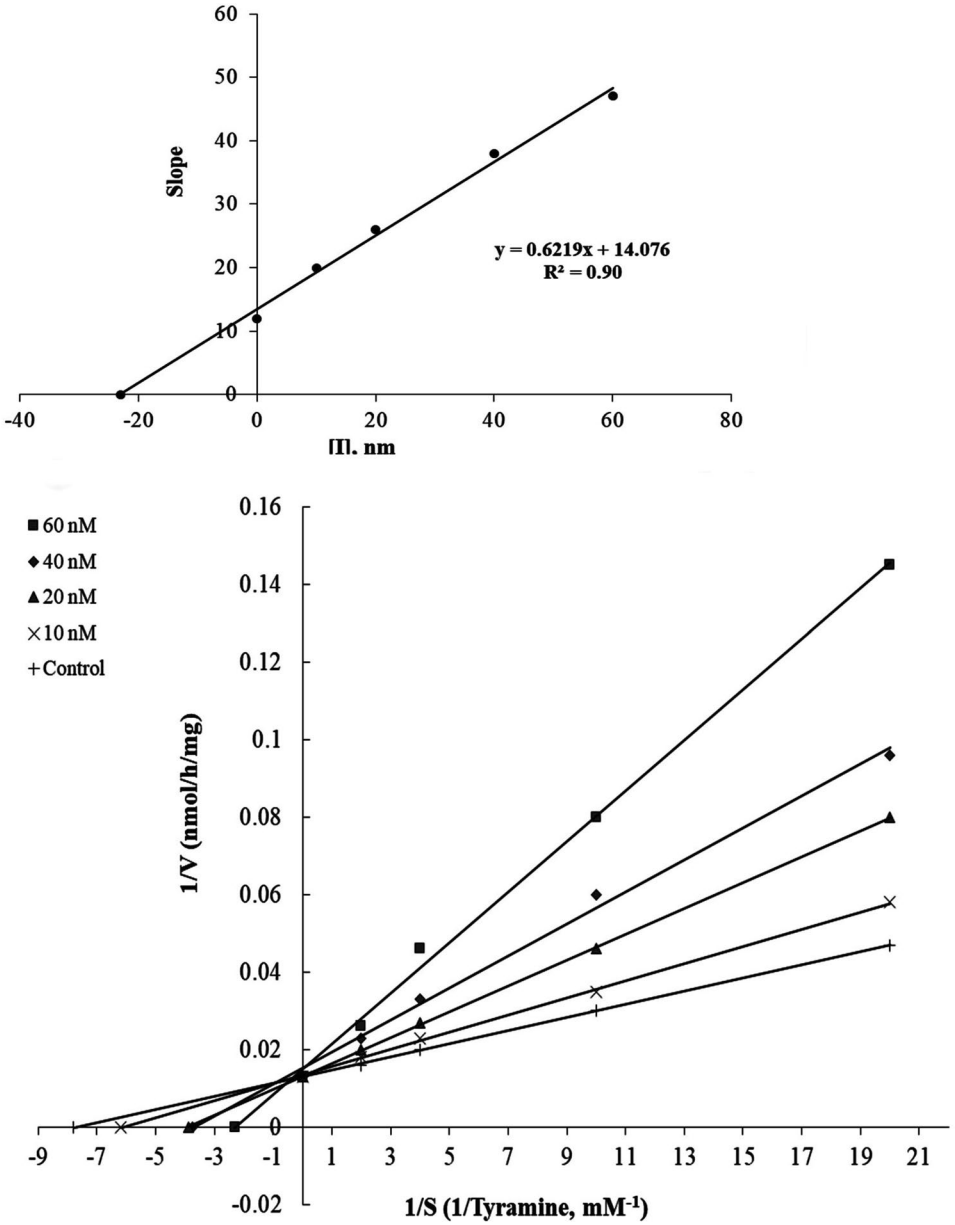

Fig. 1 The first graph shows Lineweaver–Burk plots for the inhibition of hMAO-B by compound **4b**. Inhibitor concentrations are shown at the left. *v* velocity (nmol/h/mg protein). *S* p-Tyramine (mM). From the second graph, Ki was found to be 0.023 µM

showed the highest permeability suggesting that it may cross the BBB easily and reach the biological targets located in the CNS, which is highly consistent with our design strategy.

Compounds were dissolved in DMSO at a concentration of 5 mg/ml and diluted with phosphate buffer solution/ethanol (70:30) to give a 25 µg/ml concentration. Final concentration was 100 µg/ml. Results are expressed as the SEM of three separate experiments. Values for the standard drugs were obtained from the reference by Di et al. [34].

Cytotoxicity

In vitro cytotoxicity of the synthesized pyridazinone derivatives were tested at three different concentrations (1–25 µM) (Table 5). The results showed that these compounds were not toxic to hepatic cells at 1 µM and 5 µM concentrations. Compounds, except **4f**, did not have any cytotoxicity at 25 µM concentration.

Molecular docking

The phenyl ring in the structure of the highest active compound **4b** interacted with π–π cation and with TRP 119 and PHE 103 in the active site of the enzyme. The hydrazine (NH_2–NH–) group of compound **4b** also interacted via hydrogen bonds with PRO102 and GLU84 and carbonyl (C = O) groups with TYR 326 (Fig. 2).

Table 3 Reversibility of the inhibition of hMAO isoforms by synthesized pyridazinone derivatives

Compounds incubated with hMAO isoforms	hMAO-A activity before dialysis (%)	hMAO-A activity after dialysis (%)	hMAO-B activity before dialysis (%)	hMAO-B activity after dialysis (%)	Reversibility
4a	85.01 ± 3.00	95.45 ± 2.35	20.14 ± 1.06	98.00 ± 2.63	Reversible
4b	87.00 ± 2.25	97.60 ± 3.06	12.66 ± 1.00	97.22 ± 2.85	Reversible
4c	80.26 ± 2.59	97.00 ± 2.85	31.22 ± 2.70	98.14 ± 2.44	Reversible
4d	85.22 ± 2.33	96.89 ± 2.90	29.60 ± 1.87	98.06 ± 2.37	Reversible
4e	79.90 ± 2.61	95.05 ± 3.07	39.0 ± 2.48	97.56 ± 2.13	Reversible
4f	79.90 ± 3.77	94.79 ± 2.66	39.75 ± 1.96	95.77 ± 2.29	Reversible
Moclobemide	31.11 ± 1.90	98.54 ± 2.61	81.55 ± 1.96	97.00 ± 2.62	Reversible
Selegiline	81.26 ± 1.79	97.00 ± 2.04	42.90 ± 1.87	45.55 ± 1.74	Irreversible
Lazabemide	91.26 ± 1.67	97.50 ± 2.55	13.00 ± 1.01	96.87 ± 2.97	Reversible
Control	100 ± 0.00	100 ± 0.00	100 ± 0.00	100 ± 0.00	–

*Each value represents the mean ± SEM ($n = 3$). Control: without inhibitor

Table 4 Experimental permeability (Pe 10^{-6} cm s^{-1})) in the PAMPA-BBB assay for standard drugs used in the validation of the assay and for the synthesized pyridazinone derivatives

Compounds	Bibliography Pe ($\times 10^{-6}$ cm s^{-1})	Experimental Pe ($\times 10^{-6}$ cm s^{-1})	Prediction
Testosterone	**17.0**	**16.11 ± 1.02**	**CNS +**
Verapamil	**16.0**	**15.55 ± 1.11**	**CNS +**
β-estradiol	**12.0**	**11.33 ± 0.98**	**CNS +**
Progesterone	**9.3**	**9.13 ± 0.29**	**CNS +**
Corticosterone	**5.1**	**4.78 ± 0.30**	**CNS +**
Piroxicam	**2.5**	**2.40 ± 0.12**	**CNS +/–**
Hydrocortisone	**1.8**	**1.78 ± 0.09**	**CNS–**
Lomefloxacin	**1.1**	**1.07 ± 0.08**	**CNS–**
Dopamine	**0.2**	**0.22 ± 0.01**	**CNS–**
4a		12.88 ± 0.99	CNS +
4b		15.27 ± 0.75	CNS +
4c		10.55 ± 0.96	CNS +
4d		11.27 ± 0.84	CNS +
4e		9.55 ± 0.68	CNS +
4f		7.11 ± 0.43	CNS +

To interpret the interactions, the interaction of the inhibitor with the active site of the enzyme is shown by compound **4b**. Docking studies have shown that compound **4b** is near the FAD cofactor in the active binding site of the enzyme (Fig. 3).

Docking studies showed that **4b** is bound to the catalytic site of 4A79 with high affinity (Table 6).

In Silico ADMET prediction

All calculated descriptive properties of **4a–4f** were calculated within the recommended value ranges (Table 7 and Table S1–S5). QPlogPo/w values showed that the synthesized compounds have an ideal lipophilicity other than compound **4e** (0.9). The QPlogPo/w value of Compound 4e was quite low due to the polar groups it carries unlike other compounds. According to the results of the intestinal barrier (QPPCaco) and blood–brain barrier (QPPMDCK) calculated for the **4a–4f** compounds, other than **4e**, especially compounds **4b** and **4c**, showed very good permeability. A very low blood–brain barrier passage is envisaged for compound **4e** with a QPPMDCK of 35.8. This also coincides with the experimentally calculated blood–brain barrier transition. Oral absorption values of the compounds were also predicted to be quite good except for compound **4e** (67%) with values of 80% or more. As a result, according to the estimated ADMET study results, all compounds comply with Lipinski's five rules and Jorgensen's 3 s rule.

Table 5 In vitro cytotoxicity of synthesized pyridazinone derivatives

Code	% Viability		
	0.25 µM	0.5 µM	1 µM
4a	77.36 ± 1.20	71.06 ± 1.15	69.30 ± 1.45
4b	83.28 ± 2.72	80.26 ± 1.45	79.04 ± 0.68
4c	76.42 ± 3.18	75.00 ± 1.73	73.46 ± 1.33
4d	80.14 ± 1.15	79.18 ± 2.84	80.05 ± 0.57
4e	79.66 ± 0.88	76.26 ± 2.96	69.36 ± 2.18
4f	74.02 ± 2.08	70.24 ± 1.45	62.00 ± 1.52 *

Data are expressed as mean ± SEM ($n = 3$). Cell viability is expressed as a percentage of the control value. $p < 0.05$ is considered as statistically significant (*$p < 0.05$ vs. control)

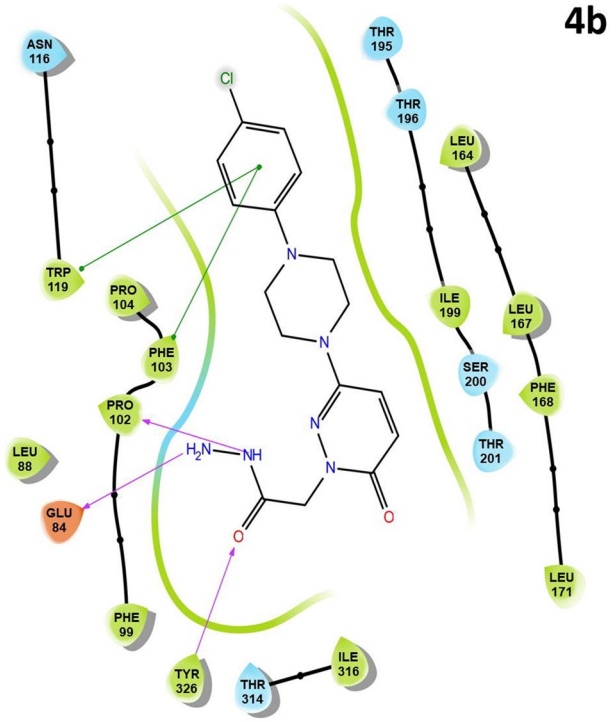

Fig. 2 Superimposition of the binding modes of **4b** on MAO-B (4A79) catalytic site obtained from Glide

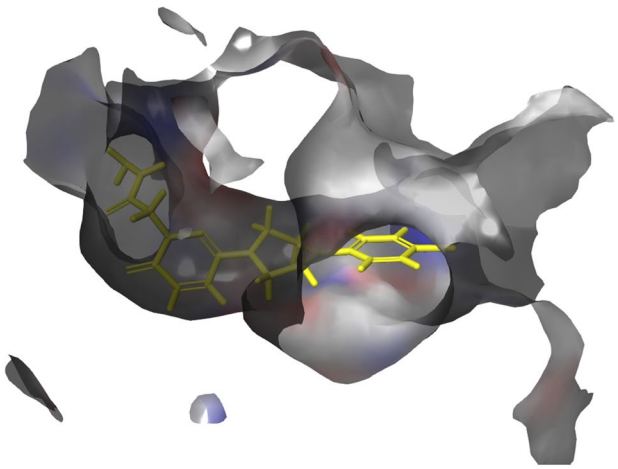

Fig. 3 Binding of compound **4b** to the MAO-B binding cavity

Discussion

Biological activity

In the present study, six pyridazinone derivatives were synthesized to examine the relationship between the structure and activity of the compounds. For this purpose, phenyl, substituted phenyl, ethoxy carbonyl and benzyl groups were attached to the fourth position of piperazine or piperidine rings located at the sixth position of the pyridazinone structure.

Table 6 Molecular docking binding scores and binding interactions of **4a–f** within the MAO-B (4A79) active site

Compound	Docking score	
	Glide	AutoDock
4a	−8.156	−9.52
4b	−8.54	−9.75
4c	−7.970	−9.5
4d	−8.073	−9.46
4e	−7.383	−8.32
4f	−8.192	−7.87

MAO isoforms are described earlier to differ in their oligomerization architecture and structures of their active sites. The active sites of the MAOs consist of a hydrophobic cavity located in front of the flavin cofactor. The only hydrophilic section is near the flavin and is required for recognition and directionality of the substrate amine functionality. This hydrophilic region plays a key role in substrate binding [44]. The binding of substrates or inhibitors to hMAO-B involves an initial negotiation of a protein loop located near the membrane surface and two hydrophobic cavities called as "entrance cavity" and "active site cavity" [45, 46].

It seems that pyridazinone, the main skeleton which is present in the structure of this series and the existence of the piperazine or piperidine ring linked to the pyridazinone seems to be necessary and important for the interaction of molecules with hMAO isoforms. Compounds **4a**, **4b**, **4c** and **4d** which are bearing phenyl substitution at piperazine ring inhibited hMAO-B potently via low K_i values (0.055 ± 0.020, 0.022 ± 0.001, 0.050 ± 0.002 and 0.061 ± 0.003 μM, respectively). Compound **4e**, which is carrying ethoxy carbonyl group substituted to piperazine ring also inhibited hMAO-B ($K_i = 0.744 \pm 0.030$ μM), however, inhibitory potency of compound **4e** was found to be lower than that of compounds **4a**, **4b**, **4c** and **4d** suggesting that phenyl substitution at piperazine ring enhances the hMAO-B inhibitory potency. Piperazine ring linked to pyridazinone skeleton appears to be essential for better hMAO-B inhibitory activity in this series since compound **4f**, which is having piperidine ring linked to pyridazinone, inhibited hMAO-B less potently ($K_i = 0.997 \pm 0.043$ μM). Compound 4f exhibited no selectivity towards hMAO isoforms whereas compounds **4a**, **4b**, **4c**, **4d** and **4e** which are having piperazine ring linked to pyridazinone inhibited hMAO-B selectively suggesting that piperazine ring linked to pyridazinone increases the selectivity of the compound towards hMAO-B isoform (Table 2).

Among the compounds which possess piperazine ring attached to the pyridazinone backbone, compound **4b** was found as the most effective MAO-B inhibitor, bearing

Table 7 Some pharmacokinetic parameters important for good oral bioavailability of compound **4a**–**4f**

Compounds	Percent human oral absorption	QPPMDCK	QPlogBB	MV	miLog P	TPSA	Drug likeness model score
	–	–	**−3 < < −1**	–	**≤ 5**	–	–
4a	79.8	94.0	−1.3	297.06	1.896	96.49	−0.17
4b	83.4	252.0	−1.2	310.59	2.407	96.49	−0.20
4c	85.7	526.1	−1.0	324.13	2.809	96.49	−0.21
4d	80.5	126.5	−1.3	301.99	2.021	96.49	−0.19
4e	67.1	35.8	−1.9	286.98	0.904	122.8	−0.12
4f	84.5	104.3	−1.3	317.90	2.564	93.26	−0.08

Percent human oral absorption predicted human oral absorption on 0 to 100% scale. The prediction is based on a quantitative multiple linear regression model. > 80% is high < 20% is poor. *QPPMDCK* predicted apparent MDCK cell permeability in nm/sec. MDCK cells are considered to be good mimics of the blood–brain barrier

4-chlorophenyl ring as R group at the piperazine ring. This compound ($K_i = 0.022 \pm 0.001$ μM) inhibited hMAO-B which indicates that the compound 4b is more effective than selegiline, ($K_i = 0.220 \pm 0.013$ μM). The selectivity of compound **4b** towards hMAO-B also was found to be the highest one (SI = 206.82) among the synthesized pyridazinone derivatives. SI value of compound **4b** appeared to be much better than that of selegiline (SI = 77.27). It has been postulated that halogen substituents in the phenyl ring enhances the MAO-B inhibition since halogen substituents improve the steric packing of small-molecules through Vander Waals interactions which facilitates binding of the derivatives to the hydrophobic active site of hMAO-B [47].

Our experimental study showed that compound **4c**, which carries 3,4-dichlorophenyl substitution at *R* position of pyridazinone moiety has also been found as a potent hMAO-B inhibitor with a K_i value of 0.050 ± 0.002 μM which makes it as more potent than selegiline. However, the hMAO-B inhibitory potency of compound **4c** appeared to be lower than that of the compound **4b** suggesting that the substitution of second chloride in phenyl ring decreases the inhibitory potency of the pyridazinones possibly causing the increase of the distance between the compound and the residues located in the region which is associated with activity. This substitution also caused a decrease in the selectivity of the compound **4c** towards hMAO-B (SI = 36.40).

Compound **4d**, which is carrying 2-fluorophenyl ring as *R* group at the piperazine ring also inhibited hMAO-B. However, inhibitory potency and the selectivity towards hMAO-B of this compound ($K_i = 0.061 \pm 0.003$ μM; SI = 35.52) were lower than those of the compounds **4b** and **4c** which are having chloride substitutions at phenyl ring possibly due to the relatively weak interaction of the fluoride atom with the amino acids located in the region associated with activity or the steric hindrance of fluoride. Compound **4e**, which is bearing ethoxy carbonyl group as *R* group at the piperazine ring inhibited hMAO-B selectively, but its inhibitory potency and selectivity towards hMAO-B (SI = 5.67) were found to be worse than those of compounds carrying phenyl ring as *R* group.

Reversibilty

The encouraging therapeutic effects of reversible, selective and competitive MAO inhibitors has prompted the researchers in the last years to investigate novel, selective and reversible drug candidates with no tyramine pressure response. Since the irreversible clinical use of MAO inhibitors is reported to be due to their serious cardiovascular or gastrointestinal side effects, current studies are mostly focused on the discovery of highly selective and reversible ones [48]. We describe here a series of pyridazinone derivaties as potent, selective and reversible inhibitors of hMAO-B which may have considerable advantages compared to irreversible inhibitors possessing serious pharmacological side effects.

Molecular docking

Compound **4a** carrying a non-substituted phenyl ring reacted *π*–*π* cation and with TRP 119 and PHE 103 in regions associated with activity, like compound **4b**. NH group also forms hydrogen bonds with TYR 326. Compound **4d** bearing fluorine substituent at second position instead of chlorine in the phenyl ring reacted via *π*–*π* cation interaction with TRP 119 and PHE 103 and hydrogen bonds with NH_2 group and TYR 326 in a similar manner to compound **4b**. The fluorine in the structure of 4d did not interact with any residues in region associated with activity of the enzyme, but caused a change in the conformation of the molecule. Due to this conformational change, the molecule could not form make hydrogen bonds with PRO102 and GLU84. Decrease in activity of compound 4d can be explained by loss of interaction with PRO102 and GLU84 in the active site of the enzyme. The structural difference of compound **4c** from compound **4b** is

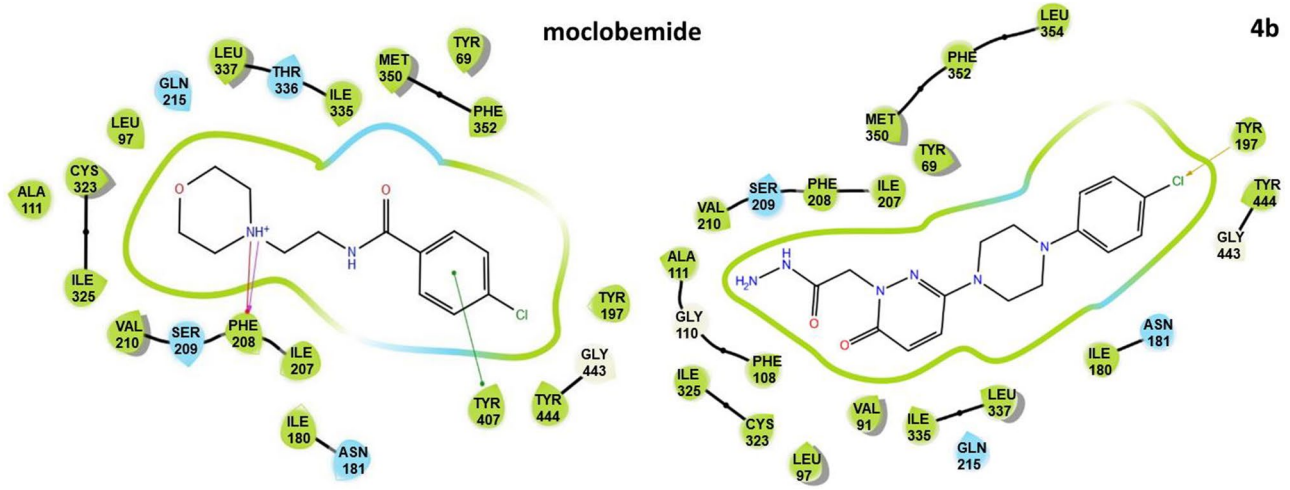

Fig. 4 Superimposition of the binding modes of Moclobemide and **4b** on MAO-A (2Z5X) catalytic site obtained from Glide

that it contains an additional chlorine substituent in the third position. The chlorine atoms in the structure of **4c** did not interact directly with the residues in the active site of the enzyme. The interaction of TRP 119 and PHE 103, which we think is related to activity along with the addition of an extra chlorine atom to the structure, has not been lost; however, the interaction of PRO102, GLU84 and TYR 326, has disappeared. The activity is, therefore, thought to be reduced.

In the compound **4e**, unlike the other compounds, there is no phenyl ring. Therefore, the interaction of TRP 119 and PHE 103 with π–π cation was eliminated and the activity was significantly decreased. In addition, as a result of conformational changes, the hydrazide substituent of the molecule bonded only with TYR 326 via hydrogen bonding. Compound **4f**, in contrast to other compounds, carries piperidine instead of piperazine ring. Furthermore, the benzyl group is attached to position four of the piperidine ring. The introduction of a carbon atom between the piperidine and the phenyl ring changed the planarity of the molecule. As a result of this conformational change, the phenyl ring was removed from the residues, TRP 119 and PHE 103, which were important for activity and could not interact. In addition, the interaction of PRO102, GLU84 and TYR 326 disappeared and activity was significantly reduced.

The synthesized compounds showed no selective inhibitory properties against MAO-A. To explain the reason for this low selectivity, the interaction of moclobemide, which is used as a reference compound in activity studies, with the active site of the enzyme 2Z5X was also investigated by docking studies. Figure 3 shows that Moclobemide interacts with the hydrogen bonding and π-cation with PHE208 and π–π cation with TYR407. In addition, the molecule was found to have polar interaction with TYR444, ILE207, VAL209 and hydrophobic interaction with SER209 and GLN215 in the active site of the enzyme (Fig. 4).

Conclusion

In recent years pyridazinones has become the subject of a large number of research due to their wide spectrum of biological activities such as analgesic, antiinflammatory, antidepressant, antihypertensive, antithrombotic, diuretics and anti-HIV [49]. The pyridazinone derivatives bearing hydrazide moiety were synthesized and their human monoamine oxidase (hMAO) inhibitory activities were evaluated by molecular docking studies by in silico ADME prediction and in vitro biological screening tests. Most of the synthesized compounds inhibited hMAO-B selectively except compound **4f**. Compounds **4a–4e** inhibited hMAO-B selectively and reversibly in a competitive mode. Compound **4b**, having 4-chlorophenyl ring as *R* group attached to piperazine moiety was found to be the most potent ($k_i = 0.022 \pm 0.001$ μM) and selective (SI ($Ki_{\text{hMAO-A/hMAO-B}}$) = 206.82) hMAO-B inhibitor in synthesized compounds.

As a result of the docking studies, the MAO-B inhibitor effect on the synthesized compounds was closely related to the interaction of the enzyme with TRP 119, PHE 103, PRO102, GLU84 and TYR 326 residues. The pyridazinone ring and hydrazide group in the structure of the compounds are important factors in the placement of the compounds in the enzyme active site. In silico ADMET prediction studies showed that the compounds were drug like in terms of most of the physicochemical parameters and they possessed generally favourable pharmacokinetic properties except their hERG inhibition potential.

In addition, the compliance with Lipinski's five rules is very important for the compounds to be drugs, and all of the compounds we synthesized comply with. Within the scope of this information, the compounds are considered to be potentially selective MAO-B inhibitors.

Acknowledgements This study was funded by Inonu University Scientific Researches Unit. (Project no: 2011/80).

Compliance with ethical standards

Conflict of interest The authors have declared no conflicts of interest.

References

1. Kumar B, Prakash V, Kumar V. A perspective on monoamine oxidase enzyme as drug target: challenges and opportunities. Curr Drug Targets. 2017;18:87–97.
2. Bortolato M, Chen K, Shih JC. Monoamine oxidase inactivation: from pathophysiology to therapeutics. Adv Drug Deliv Rev. 2008;60:1527–33.
3. Finberg JPM, Rabey JM. Inhibitors of MAO-A and MAO-B in psychiatry and neurology. Front Pharmacol. 2016;7:340.
4. Evranos-Aksoz B, Ucar G, Tas ST, Aksoz E, Yelekci K, Erikci A, et al. New human monoamine oxidase A inhibitors with potential anti-depressant activity: design, synthesis, biological screening and evaluation of pharmacological activity. Comb Chem High Throughput Screen. 2017;20(6):461–73.
5. Gunal SE, Tuncel ST, Gokhan-Kelekci N, Ucar G, Dursun BY, Sag-Erdem S, et al. Asymmetric synthesis, molecular modeling and biological evaluation of 5-methyl-3-aryloxazolidine-2,4-dione enantiomers as monoamine oxidase (MAO) inhibitors. Bioorg Chem. 2018;77:608–18.
6. Mathew B, Ucar G, Rapheal C, Mathew GE, Joy M, Machaba KE, et al. Characterization of thienylchalcones as hMAO-B inhibitors: synthesis, biochemistry and molecular dynamics studies. Chem Select. 2017;2(34):11113–9.
7. Pathak A, Srivastava AK, Singour PK, Gouda P. Synthetic and natural monoamine oxidase inhibitors as potential lead compounds for effective therapeutics. Cent Nerv Syst Agents Med Chem. 2016;16(2):81–97.
8. Chimenti F, Bolasco A, Secci D, Chimenti P, Granese A, Carradori S, et al. Investigations on the 2-thiazolylhydrazyne scaffold: synthesis and molecular modeling of selective human monoamine oxidase inhibitors. Bioorg Med Chem. 2010;18:5715–23.
9. Entzeroth M, Ratty AK. Monoamine oxidase inhibitors—revisiting a therapeutic principle. Open J Depression. 2017;6:31–68.
10. Kumar B, Sheetal Mantha AK, Kumar V. Recent developments on the structure–activityrelationship studies of MAO inhibitors and their role in different neurological disorders. RSC Adv. 2016;6:42660–83.
11. Secci D, Bolasco A, Carradori S, Ascenzio MD, Nescatelli R, Yanez M. Recent advances in the development of selective human MAO-B inhibitors: (hetero)arlylidene-(4-substituted-thiazol-2-yl) hydrazines. Eur J Med Chem. 2012;58:405–17.
12. Binda C, Wang J, Pisani L, Caccia C, Carotti A, Salvati P, et al. Structures of human monoamine oxidase B complexes with selective noncovalent inhibitors: safinamide and coumarin analogs. J Med Chem. 2007;50(23):5848–52.
13. Can NÖ, Osmaniye D, Levent S, Sağlık BN, Korkut B, Atlı Ö, et al. Design, synthesis and biological assessment of new thiazolylhydrazine derivatives as selective and reversible hMAO-A inhibitors. Eur J Med Chem. 2018;144:68–81.
14. Akhtar W, Shaquiquzzaman M, Akhter M, Verma G, Khan MF, Alam MM. The therapeutic journey of pyridazinone. Eur J Med Chem. 2016;123:256–81.
15. Geng P-F, Liu X-Q, Zhao T-Q, Wang C-C, Li Z-H, Zhang J, et al. Design, synthesis and in vitro biological evaluation of novel [1,2,3] triazolo[4,5-d]pyrimidine derivatives containing a thiosemicarbazide moiety. Eur J Med Chem. 2018;146:147–56.
16. Banerjee PS. Various biological activities of pyridazinone ring derivatives. Asian J Chem. 2011;23(5):1905–10.
17. Nagle P, Pawar Y, Sonawane A, Bhosale S, More D. Docking simulation, synthesis and biological evaluation of novel pyridazinone containing thymol as potential antimicrobial agents. Med Chem Res. 2014;23:918–26.
18. Utku S, Gökçe M, Aslan G, Bayram G, Ülger M, Emekdaş G, et al. Synthesisand in vitroantimycobacterialactivities of novel 6-substituted-3(2*H*)-pyridazinone-2-acetyl-2(substituted/nonsubstituted acetophenone) hydrazone. Turk J Chem. 2011;35:331–9.
19. Şahin MF, Badıçoglu B, Gökçe M, Küpeli E, Yeşilada E. Synthesis and analgesic and antiinflammatory activity of methyl [6-substitue-3(*2H*)- pyridazinone-2-yl]acetate derivatives. Arch Pharm. 2004;33:445–52.
20. Siddiqui AA, Mishra R, Shaharyar M. Synthesis, characterization and antihypertensive activity of pyridazinone derivatives. Eur J Med Chem. 2010;45:2283–90.
21. Siddiqui AA, Mishra R, Shaharyar M, Husain A, Rashid M, Pal P. Triazole incorporated pyridazinones as a new class of antihypertensive agents: design, synthesis and in vivo screening. Bioorg Med Chem Lett. 2011;21:1023–6.
22. Yamali C, Ozan GH, Kahya B, Çobanoğlu S, Şüküroğlu MK, Doğruer DS. Synthesis of some 3(2*H*)-pyridazinone and 1(*2H*)-phthalazinone derivatives incorporating aminothiazole moiety and investigation of their antioxidant, acetylcholinesterase, and butyrylcholinesterase inhibitory activities. Med Chem Res. 2015;24:1210–7.
23. Rathish IG, Javed K, Ahmad S, Bano S, Alam MS, Akhter M, et al. Synthesis and evaluation of anticancer activity of some novel 6-aryl-2-(*p*-sulfamylphenyl)-pyridazin-3(*2H*)-ones. Eur J Med Chem. 2012;49:304–9.
24. El-Ghaffar NFA, Mohamed MK, Kadah MS, Radwan AM, Said GH, Abd SN. Synthesis and anti-tumor activities of some new pyridazinones containing the 2-phenyl-1*H*-indolyl moiety. J Chem Pharm Res. 2011;3(3):248–59.
25. Malinka W, Kaczmarz M, Redzicka A. Antitumor in vitro evaluation of certain derivatives of pyrido-1,2-thiazines. Acta Pol Pharm. 2014;61(Suppl):100–2.
26. Utku S, Gökçe M, Orhan İ, Şahin MF. Synthesis of novel 6-substituted-3(*2H*)-pyridazinone-2-acetyl-2-(substituted/-nonsubstituted benzal) hydrazone derivatives and acetylcholinesterase and butyrylcholinesterase inhibitory activities in vitro. Arzneimittelforschug. 2011;61:1–7.
27. Önkol T, Gökçe M, Orhan İ, Kaynak F. Design, synthesis and evaluation of some novel 3(2*H*)-pyridazinone-2-yl acetohydrazides as acetylcholinesterase and butyrylcholnesterase inhibitors. Org Commun. 2014;6(1):55–67.
28. Özdemir Z, Gökçe M, Karakurt A. Synthesis and analgesic, antiinflammatory and antimicrobial evaluation of 6-substituted-3(2*H*)-pyridazinone-2-acetyl-2-(substitutedbenzal)hydrazine derivatives. FABAD J Pharm Sci. 2012;37(2):111–22.
29. Özdemir Z, Yılmaz H, Sarı S, Karakurt A, Şenol FS, Uysal M. Design, synthesis, and molecular modeling of new 3(2*H*)-pyridazinone derivatives as acetylcholinesterase/butyrylcholinesterase inhibitors. Med Chem Res. 2017;26(10):2293–308.
30. Yáñez M, Fraiz N, Cano E, Orallo F. Inhibitory effects of cis- and trans-resveratrol on noradrenaline and 5-hydroxytryptamine

uptake and on monoamine oxidase activity. Biochem Biophys Res Commun. 2006;344:688–95.
31. Chimenti F, Maccioni E, Secci D, Bolasco A, Chimenti P, Granese A, et al. Synthesis, stereochemical identification, and selective inhibitory activity against human monoamine oxidase-B of 2-methylcyclohexylidene-(4-arylthiazol-2-yl)hydrazones. J Med Chem. 2008;51:4874–80.
32. Chimenti F, Carradori S, Secci D, Bolasco A, Bizzarri B, Chimenti P, et al. Synthesis and inhibitory activity against human monoamine oxidase of N1-thiocarbamoyl-3, 5-di (hetero) aryl-4, 5-dihydro-(1H)-pyrazole derivatives. Eur J Med Chem. 2010;45(2):800–4.
33. Jhala DD, Chettiar SS, Singh JK. Optimization and validation of an in vitro blood brain barrier permeability assay using artificial lipid membrane. J Bioequiv Availab. 2012;S14:1–5.
34. Di L, Kerns EH, Fan K, McConnell OJ, Carter GT. High throughput artificial membrane permeability assay for blood–brain barrier. Eur J Med Chem. 2003;38(3):223–32.
35. Wu CF, Bertorelli R, Sacconi M, Pepeu G, Consolo S. Decrease of brain acetylcholine release in aging freely-moving rats detected by microdialysis. Neurobiol Aging. 1988;9:357–61.
36. Banks JL, Beard HS, Cao YX, Cho AE, Damm W, Farid R, et al. Integrated modeling program, applied chemical theory (IMPACT). J Comput Chem. 2005;26:1752–80.
37. Berman HM, Westbrook J, Feng Z, Gilliland G, Bhat TN, Weissig H, et al. The protein data bank. Nucleic Acids Res. 2000;28:235–42.
38. Shelley JC, Cholleti A, Frye LL, Greenwood JR, Timlin MR, Uchimaya M. Epik: a software program for pK(a) prediction and protonation state generation for drug-like molecules. J Comput Aided Mol Des. 2007;21:681–91.
39. Friesner RA, Banks JL, Murphy RB, Halgren TA, Klicic JJ, Mainz DT, et al. Glide: a new approach for rapid, accurate docking and scoring. 1. Method and assessment of docking accuracy. J Med Chem. 2004;47(7):1739–49.
40. Friesner RA, Murphy RB, Repasky MP, Frye LL, Greenwood JR, Halgren TA, et al. Extra precision glide: docking and scoring incorporating a model of hydrophobic enclosure for protein-ligand complexes. J Med Chem. 2006;49:6177–96.
41. Halgren TA, Murphy RB, Friesner RA, Beard HS, Frye LL, Pollard DT, et al. Glide: a new approach for rapid, accurate docking and scoring. 2. Enrichment factors in database screening. J Med Chem. 2004;47(7):1750–9.
42. Morris G, Huey R, Lindstrom W, Sanner MF, Belew RK, Goodsell DS, et al. AutoDock4 and AutoDockTools4: automated docking with selective receptor flexibility. J Comput Chem. 2009;30(16):2785–91.
43. Badavath VN, Ucar G, Sinha BN, Mondal SK, Jayakrapash V. Monoamine oxidase inhibitory activity of novel pyrazoline analogues: curcumin based design and synthesis-II. Chem Select. 2016;1(18):5879–84.
44. Binda C, Li M, Hubálek F, Restelli N, Edmondson DE, Mattevi A. Insights into the mode of inhibition of human mitochondrial monoamine oxidase B from high-resolution crystal structures. PNAS. 2003;11(17):9750–5.
45. Iacovino LG, Magnani F, Binda C. The structure of monoamine oxidases: past, present, and future. J Neural Transm. 2018;125(11):1567–79.
46. Kumar B, Sheetal Mantha AK, Kumar V, Rauhamäki S, Postila PA, Niinivehmas S, et al. Synthesis, biological evaluation and molecular modeling studies of phenyl-/benzhydrylpiperazine derivatives as potential MAO inhibitors. Bioorg Chem. 2018;77:252–62.
47. Rauhamäki S, Postila PA, Niinivehmas S, Kortet S, Schildt E, Pasanen M, et al. Structure-activity relationship analysis of 3-phenylcoumarin-based monoamine oxidase B inhibitors. Front Chem. 2018;6:41.
48. Ramsay RR, Tipton KF. Assessment of enzyme inhibition: a review with examples from the development of monoamine oxidase and cholinesterase inhibitory drugs. Molecules. 2017;22(7):1192.
49. Seth S, Sharma A, Raj D. Pyridazinones: a wonder nucleus with scaffold of pharmacological activities. Am J Biol Pharm Res. 2014;1(3):105–16.